Optics Letters

Ultra-compact and low-threshold thulium microcavity laser monolithically integrated on silicon

Zhan Su,[1,*] Nanxi Li,[1,2] E. Salih Magden,[1] Matthew Byrd,[1] Purnawirman,[1] Thomas N. Adam,[3] Gerald Leake,[3] Douglas Coolbaugh,[3] Jonathan D. B. Bradley,[1,4,5] and Michael R. Watts[1,6]

[1]Research Laboratory of Electronics, Massachusetts Institute of Technology, 77 Massachusetts Avenue, Cambridge, Massachusetts 02139, USA
[2]John A. Paulson School of Engineering and Applied Sciences, Harvard University, 29 Oxford Street, Cambridge, Massachusetts 02138, USA
[3]Colleges of Nanoscale Science and Engineering, State University of New York Polytechnic Institute, 257 Fuller Road, Albany, New York 12203, USA
[4]Currently at Department of Engineering Physics, McMaster University, 1280 Main Street West, Hamilton, Ontario L8S 4L7, Canada
[5]e-mail: jbradley@mcmaster.ca
[6]e-mail: mwatts@mit.edu
*Corresponding author: zhansu@mit.edu

Received 3 October 2016; accepted 3 November 2016; posted 15 November 2016 (Doc. ID 278024); published 8 December 2016

We demonstrate an ultra-compact and low-threshold thulium microcavity laser that is monolithically integrated on a silicon chip. The integrated microlaser consists of an active thulium-doped aluminum oxide microcavity beside a passive silicon nitride bus waveguide, which enables on-chip pump-input and laser-output coupling. We observe lasing in the wavelength range of 1.8–1.9 μm under 1.6 μm resonant pumping and at varying waveguide-microcavity gap sizes. The microlaser exhibits a threshold as low as 773 μW (226 μW) and a slope efficiency as high as 24% (48%) with respect to the pump power coupled into the silicon nitride bus waveguide (microcavity). Its small footprint, minimal energy consumption, high efficiency, and silicon compatibility demonstrate that on-chip thulium lasers are promising light sources for silicon microphotonic systems.

OCIS codes: (130.3120) Integrated optics devices; (140.0140) Lasers and laser optics; (140.3948) Microcavity devices.

https://doi.org/10.1364/OL.41.005708

Thulium lasers are of significant interest because of their high efficiencies, high output powers and eye-safe emission at wavelengths ranging from 1.7 to 2.2 μm. Important applications of thulium lasers include gas sensing, free space communications, biomedicine, lidar, and nonlinear mid-infrared generation [1,2]. Thus far, ~2 μm thulium lasers have been developed on a variety of photonic platforms, including bulk crystals [3–5], glass fibers [6–9], planar and channel waveguides [10–16], and whispering-gallery microresonators [17–19].

Silicon is currently under intensive development as a platform for low-cost, energy-efficient, and high-speed integrated photonic microsystems, especially for the traditional communication wavelength bands around 1.3 and 1.5 μm. Recently, however, a considerable amount of research has been applied toward extending the operational range of silicon photonic systems beyond 1.5 μm for communications, sensing, and advanced metrology applications. In particular, there is a focus on an emerging 2 μm silicon photonics window, motivated in part by the development of low-loss photonic crystal fibers, extended-range silicon detectors, and thulium fiber amplifiers [20–22].

Since silicon itself is a poor light emitter, compact, efficient, and monolithic silicon-based light sources operating near 2 μm are desirable. However, despite their high performance in other platforms and the realization of 1.5 μm erbium- and other rare-earth-doped glass lasers on silicon [23–26], silicon-integrated thulium lasers, to date, are minimally explored. While thulium microlasers have been demonstrated on silicon chips [27,28], their designs required an off-chip fiber for pump coupling and laser emission. To implement thulium microlasers within silicon photonic microsystems, they must be co-integrated with on-chip waveguides and fabricated using silicon-compatible methods.

In this Letter, we report on thulium-doped microcavity lasers co-integrated with silicon nitride bus waveguides on silicon. The 200 μm diameter thulium microlasers are enabled by a novel high quality factor (Q-factor) microcavity design, which includes two silicon nitride layers and a silicon dioxide trench filled with thulium-doped aluminum oxide (Al_2O_3:Tm^{3+}). We show a sub-milliwatt threshold and high-efficiency lasing around 1.8–1.9 μm under resonant pumping at 1.6 μm. The entire fabrication process is silicon compatible and allows for the co-integration of such lasers with other silicon-based photonic devices and microsystems.

We fabricated the thulium microcavity lasers using a 300 mm CMOS foundry with a 65 nm technology node. A similar fabrication process and microlaser design with ytterbium applied as dopants is explained in detail in [26]. The feature dimensions were changed in this Letter to accommodate both the pump and the lasing wavelengths of thulium ions.

Figure 1(a) shows a schematic of the microcavity laser. The cavity consists of a 15 μm wide and 4 μm deep circular trench etched into a SiO_2 cladding and filled with a 1.5 μm thick Al_2O_3:Tm^{3+} film with a thulium concentration of 2.5e20 cm^{-3}. The concentration was selected to allow for a greater gain than total cavity loss while maintaining a low laser threshold. The integrated bus waveguide is adjacent to the microcavity and consists of two 200 nm thick Si_3N_4 layers separated by a vertical 100 nm SiO_2 gap. Because the upper Si_3N_4 layer also acts as an etch stop during the microcavity trench etch [25,26], small (~300 nm wide) pieces of Si_3N_4 remain at the edge of the trench. Based on finite element mode solver calculations, we selected the outer diameter of the microcavity to be 200 μm to minimize bending loss and support high quality factor lasing modes around 1.8–1.9 μm. We also selected a nominal Si_3N_4 bus waveguide width of 915 nm for the phase-matched coupling of pump light at wavelengths around 1.6 μm. We fabricated devices with waveguide-microcavity gap sizes of 0.2–1.3 μm to investigate a range of coupling strengths. A cross-sectional drawing of the laser structure (taken at a location indicated by the green dashed line) is shown in the inset of Fig. 1(a). The deep trench has an angle of ~85°, while the Al_2O_3:Tm^{3+} film in the middle of the trench is thicker than that along the trench edge due to the angular dependence of the reactive co-sputtering deposition process [25,26,29]. The simulated mode profiles for 1.6 and 1.8 μm wavelengths are also displayed in the inset of Fig. 1(a), showing a large overlap with the Al_2O_3:Tm^{3+} layer and pump/laser mode overlap, important for achieving optical gain and lasing [25]. Fig. 1(b) displays a top-view optical microscope image of a fabricated device.

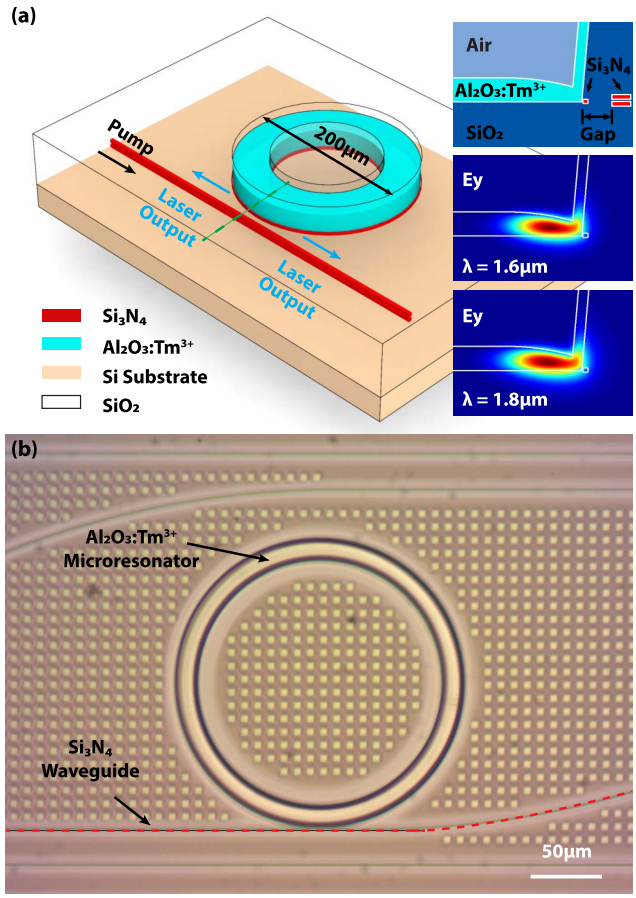

Fig. 1. (a) Schematic of an on-chip thulium microcavity laser. Inset: cross section of the laser structure and resonant mode profiles for 1.6 (pump) and 1.8 μm (laser output) wavelengths in the cavity. (b) Top-view optical microscope image of a fabricated device, showing the integrated thulium-doped aluminum oxide microresonator and silicon nitride bus waveguide (red dashed line).

We characterized the microcavity lasers using the experimental setup shown in Fig. 2(a). We coupled pump light from a narrow linewidth (100 kHz), tunable (1500–1625 nm) laser to a polarization controller to adjust the input light to transverse-magnetic (TM) polarization, and onto the chip via a tapered fiber with a coupling efficiency of –2.25 dB per facet. Due to the degeneracy of the clockwise and counter-clockwise modes inside the cavity, lasing occurs in both directions. Therefore, we coupled the laser output in the bus waveguide off chip from both sides using tapered fibers, followed by wavelength division multiplexers (WDMs) to separate the input/residual pump light, and then collected it at optical spectrum analyzers (OSAs) to measure the optical power and emission spectrum. We measured the transmitted pump power using an optical power meter.

The transmission spectrum of a device with a gap of 0.9 μm measured from 1593 to 1615 nm is shown in Fig. 3(a). Three different radial modes are marked with arrows on Fig. 3(a) around a wavelength of 1608 nm (each with a free-spectral-range of ~2 nm). Modes with the same radial order as the one marked with a red circle on Fig. 3(a) were found to provide lasing behavior as predicted by calculations taking into account the quality factor, the confinement within the gain medium, and the overlap of the pump and lasing modes. We also fabricated another set of devices with undoped Al_2O_3 as a comparison. The measured intrinsic Q-factors of doped and undoped microcavities at 1610 nm are 6.8e4 and 4.3e5, respectively.

In Fig. 3(b), we show the resonantly absorbed 1608 nm pump power versus the microcavity-waveguide gap size. With a TM input, we observed optimum pump coupling of 95% near a gap width of 0.5 μm. However, lasing did not occur for gap sizes <0.7 μm. For gap sizes below 0.7 μm, the total cavity Q-factor for lasing wavelengths ≥1.8 μm becomes too low, leading to a roundtrip net loss or a lasing threshold that is beyond the maximum output power of the tunable laser utilized in the experiment. We observed lasing behavior at waveguide-microcavity gap sizes ranging from 0.7 to 1.3 μm.

We observed the highest laser output power when resonantly pumping at a wavelength around 1608 nm, near the peak of the thulium ion $^3H_6 \rightarrow {}^3F_4$ absorption cross section. Figure 4(a) shows the total (double-sided) on-chip laser power as a function of on-chip pump power for different pump wavelengths and a gap of 0.9 μm. While it shows a similar lasing threshold for pump wavelengths from 1594 to 1614 nm, pumping around 1608 nm shows the highest slope efficiency. Figure 4(b) shows

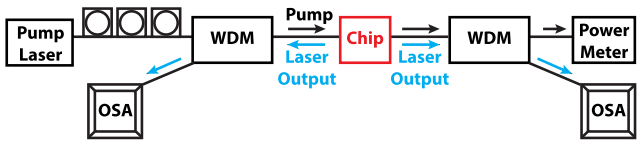

Fig. 2. Experimental setup used for thulium-doped microcavity laser measurements. A tunable laser pump light is coupled into the chip through a polarization controller and a 1.6/1.8 μm fiber WDM. The laser output is measured at the OSAs on both sides of the chip.

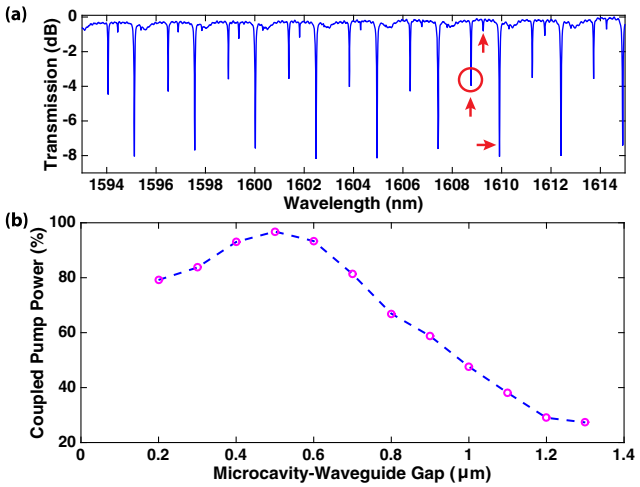

Fig. 3. (a) TM-polarized transmission spectrum for a device with a gap of 0.9 μm over the wavelength range of 1593–1615 nm, showing three clear resonant modes of different radial orders (marked by red arrows) within one free-spectral-range. The mode that leads to low-threshold lasing is marked with a red circle. (b) Coupled pump power for the pump mode circled in Fig. 3(a) in Tm-doped microcavities with a bus waveguide width of 0.915 μm and microcavity-waveguide gap sizes ranging from 0.2 to 1.3 μm. Maximum coupling occurs at gaps near 0.5 μm when the internal and external Q-factors of the resonator are matched.

the lasing thresholds and double-sided slope efficiencies under 1608 nm pumping for varying microcavity-waveguide gap sizes. A double-sided slope efficiency as high as 24% and a threshold as low as 773 μW were observed for gap sizes of 0.9 and 1.0 μm, respectively, with respect to the pump power coupled into the Si_3N_4 bus waveguide. Accounting for the cavity-coupled pump powers shown in Fig 3(b), we also plot the thresholds and slope efficiencies with respect to absorbed pump power for varying gap sizes in Fig. 4(c). We determine a maximum doublesided slope efficiency of 48% with respect to absorbed pump power for the laser device with 1.1 μm microcavity-waveguide gap size. We observed a minimum threshold of 226 μW versus absorbed pump power at the largest gap size of 1.3 μm, where the total cavity Q-factor is the highest.

Figure 5 shows laser output spectra measured on one side of the chip for microcavity-waveguide gap sizes ranging from 0.7 to 1.3 μm. We observe multi-mode lasing and laser modes spanning from 1.8 to 1.9 μm. The devices tend to lase at longer wavelengths for larger gap sizes. This trend can be explained by the gap size and wavelength dependence of the loaded cavity Q-factor, the shape of the thulium emission spectrum with its peak near 1.8 μm, and the blue-shifted Tm^{3+} absorption spectrum with respect to the emission spectrum. For smaller gap sizes (and longer wavelengths), the cavity modes have a greater coupling strength and lower Q-factor (higher roundtrip loss), making the microcavity more likely to lase on higher gain modes near the Tm^{3+} emission peak at 1.8 μm. For larger gap sizes, the Q-factor of all cavity modes increases (roundtrip loss decreases); thus, the laser output shifts to longer wavelengths where the Tm^{3+} absorption is lower, and population inversion is more easily achieved. This trend indicates that by increasing the gap width beyond 1.3 μm, longer wavelength lasing could

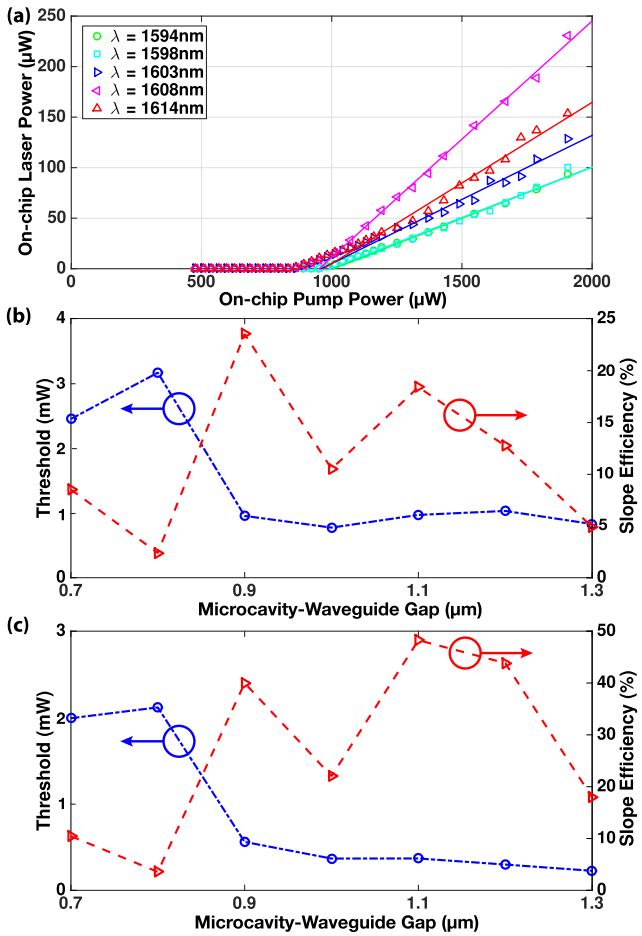

Fig. 4. (a) On-chip laser power as a function of on-chip pump power for different pump wavelengths for a device with 0.9 μm gap size, showing the highest-efficiency lasing and output power >200 μW when resonantly pumped at 1608 nm. (b) Lasing thresholds and slope efficiencies with respect to on-chip pump power for different microcavity-waveguide gap sizes. (c) Lasing thresholds and slope efficiencies with respect to absorbed power for different microcavity-waveguide gap sizes.

possibly be achieved. Further, by reducing the bus waveguide width for phase-matched pumping at shorter wavelengths, we can pump the microcavity lasers with low-cost, efficient 780 nm lasers. This can potentially lead to an even higher lasing efficiency due to "two for one" excitation via Tm^{3+}–Tm^{3+} ion cross-relaxation [3]. Finally, by adding grating features [30] and asymmetry to the current cavity design, single-mode or directional lasing [31–33] could possibly be achieved in future iterations.

In conclusion, we have demonstrated low-threshold and high-efficiency thulium-doped microcavity lasers which are monolithically integrated on a silicon photonic chip. The lasers have thresholds as low as 773 (226) μW and slope efficiencies of up to 24% (48%) versus on-chip (absorbed) pump power. By changing the waveguide-microcavity gap and resonantly pumping at 1608 nm, we show lasing in the range of 1.8–1.9 μm. In the future, optimizing the Tm^{3+} concentration, coupling strength, and cavity design can lead to even greater efficiencies, emission over a wider wavelength range across thulium's broad gain spectrum (~1.7 – 2.2 μm), single-mode operation,

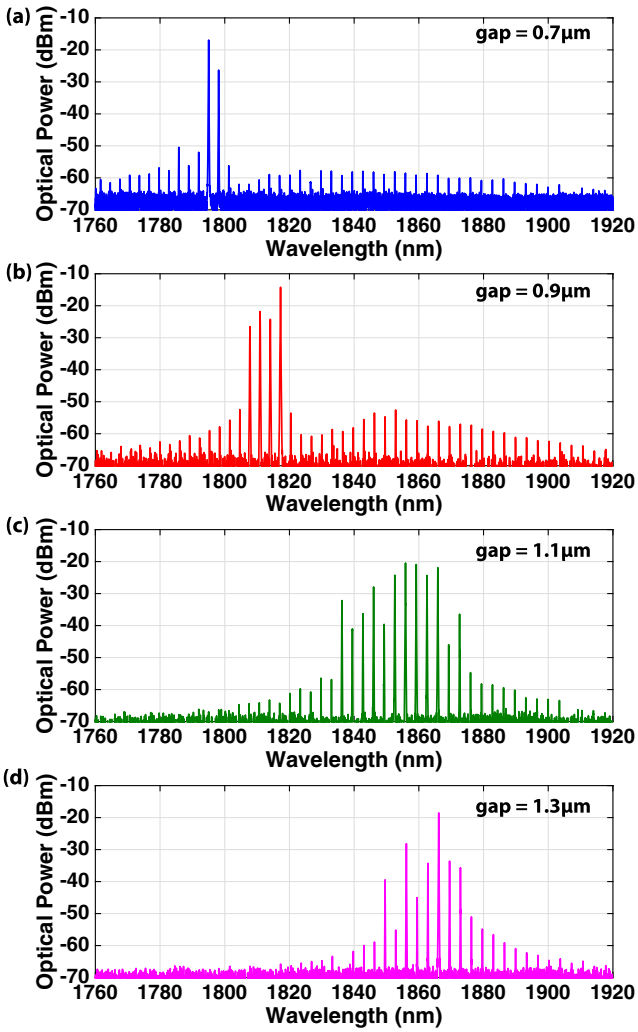

Fig. 5. Laser emission spectra under 1608 nm pumping and at microcavity-waveguide gaps of (a) 0.7, (b) 0.9, (c) 1.1, and (d) 1.3 μm, showing a shift of the laser output to longer wavelengths with the increase of microcavity-waveguide gap size.

and directionality. These results demonstrate integrated thulium lasers to be of interest as highly efficient monolithic light sources for emerging silicon-based photonic microsystems.

Funding. Defense Advanced Research Projects Agency (DARPA) (HR0011-12-2-0007, HR0011-15-C-0056).

Acknowledgment. We thank K. Broderick for his assistance and discussion on thulium-doped thin film deposition. N. Li acknowledges a fellowship from the Agency of Science, Technology, and Research (A*STAR), Singapore.

REFERENCES

1. Q. Wang, J. Geng, and S. Jiang, Opt. Eng. **53**, 061609 (2014).
2. K. Scholle, S. Lamrini, P. Koopmann, and P. Fuhrberg, in *Frontiers in Guided Wave Optics and Optoelectronics*, B. Pal, ed. (In Tech, 2010).
3. G. Huber, C. Kränkel, and K. Petermann, J. Opt. Soc. Am. B **27**, B93 (2010).
4. W. Ryba-Romanowski, R. Lisiecki, H. Jelinková, and J. Šulc, Prog. Quantum Electron. **35**, 109 (2011).
5. M. Gaponenko, N. Kuleshov, and T. Südmeyer, Opt. Express **22**, 11578 (2014).
6. D. J. Richardson, J. Nilsson, and W. A. Clarkson, J. Opt. Soc. Am. B **27**, B63 (2010).
7. S. D. Jackson, Nat. Photonics **6**, 423 (2012).
8. C. W. Rudy, M. J. F. Digonnet, and R. L. Byer, Opt. Fiber Technol. **20**, 642 (2014).
9. J. Li, Z. Sun, H. Luo, Z. Yan, K. Zhou, Y. Liu, and L. Zhang, Opt. Express **22**, 5387 (2014).
10. D. P. Shepherd, G. Kakarantzas, P. D. Townsend, D. J. B. Brinck, J. Wang, A. C. Tropper, and D. C. Hanna, Opt. Lett. **19**, 954 (1994).
11. A. Rameix, C. Borel, B. Chambaz, B. Ferrand, D. P. Shepherd, T. J. Warburton, D. C. Hanna, and A. C. Tropper, Opt. Commun. **142**, 239 (1997).
12. S. Rivier, X. Mateos, V. Petrov, U. Griebner, Y. E. Romanyuk, C. N. Borca, F. Gardillou, and M. Pollnau, Opt. Express **15**, 5885 (2007).
13. W. Bolanos, F. Starecki, A. Benayad, G. Brasse, V. Ménard, J. Doualan, A. Braud, R. Moncorgé, and P. Camy, Opt. Lett. **37**, 4032 (2012).
14. E. Cantelar, J. A. Sanz-García, G. Lifante, F. Cussó, and P. L. Pernas, Appl. Phys. Lett. **86**, 161119 (2005).
15. D. G. Lancaster, S. Gross, M. J. Withford, and T. M. Monro, Opt. Express **22**, 25286 (2014).
16. K. van Dalfsen, S. Aravazhi, C. Grivas, S. M. García-Blanco, and M. Pollnau, Opt. Lett. **39**, 4380 (2014).
17. J. Wu, S. Jiang, T. Qua, M. Kuwata-Gonokami, and N. Peyghambarian, Appl. Phys. Lett. **87**, 211118 (2005).
18. A. Pal, S. Y. Chen, R. Sen, T. Sun, and K. T. V. Grattan, Laser Phys. Lett. **10**, 085101 (2013).
19. F. Vanier, F. Côté, M. El Amraoui, Y. Messaddeq, Y.-A. Peter, and M. Rochette, Opt. Lett. **40**, 5227 (2015).
20. R. Soref, Nat. Photonics **4**, 495 (2010).
21. G. Roelkens, U. D. Dave, A. Gassenq, N. Hattasan, C. Hu, B. Kuyken, F. Leo, A. Malik, M. Muneeb, E. Ryckeboer, D. Sanchez, S. Uvin, R. Wang, Z. Hens, R. Baets, Y. Shimura, F. Gencarelli, B. Vincent, R. Loo, J. Van Campenhout, L. Cerutti, J.-B. Rodriguez, E. Tournié, X. Chen, M. Nedeljkovic, G. Mashanovich, L. Shen, N. Healy, A. C. Peacock, X. Liu, R. Osgood, and W. M. J. Green, IEEE J. Sel. Top. Quantum Electron. **20**, 394 (2014).
22. J. J. Ackert, D. J. Thomson, L. Shen, A. C. Peacock, P. E. Jessop, G. T. Reed, G. Z. Mashanovich, and A. P. Knights, Nat. Photonics **9**, 393 (2015).
23. J. D. B. Bradley and M. Pollnau, Laser Photon. Rev. **5**, 368 (2011).
24. Purnawirman, J. Sun, T. N. Adam, G. Leake, D. Coolbaugh, J. D. B. Bradley, E. Shah Hosseini, and M. R. Watts, Opt. Lett. **38**, 1760 (2013).
25. J. D. B. Bradley, E. Shah Hosseini, Purnawirman, Z. Su, T. N. Adam, G. Leake, D. Coolbaugh, and M. R. Watts, Opt. Express **22**, 12226 (2014).
26. Z. Su, J. D. B. Bradley, N. Li, E. S. Magden, P. Purnawirman, D. Coleman, N. Fahrenkopf, C. Baiocco, T. Adam, G. Leake, D. Coolbaugh, D. Vermeulen, and M. R. Watts, in *Advanced Photonics 2016 (IPR, NOMA, Sensors, Networks, SPPCom, SOF)*, OSA technical Digest (online) (Optical Society of America, 2016), paper IW1A.3.
27. S. Mehrabani and A. M. Armani, Opt. Lett. **38**, 4346 (2013).
28. H.-B. Fan, X.-S. Jiang, Y. Ding, and M. Xiao, Sci. China Phys. Mech. Astron. **58**, 114204 (2015).
29. K. Wörhoff, J. D. B. Bradley, F. Ay, D. Geskus, T. P. Blauwendraat, and M. Pollnau, IEEE J. Quantum Electron. **45**, 454 (2009).
30. A. Arbabi, S. M. Kamali, E. Arbabi, B. G. Griffin, and L. L. Goddard, Opt. Express **23**, 5335 (2015).
31. Y.-F. Xiao, C.-L. Zou, Y. Li, C.-H. Dong, Z.-F. Han, and Q. Gong, Front. Optoelectron. China **3**, 109 (2010).
32. X.-F. Jiang, Y.-F. Xiao, C.-L. Zou, L. He, C.-H. Dong, B.-B. Li, Y. Li, F.-W. Sun, L. Yang, and Q. Gong, Adv. Mater. **24**, 260 (2012).
33. X.-F. Jiang, C.-L. Zou, L. Wang, Q. Gong, and Y.-F. Xiao, Laser Photon. Rev. **10**, 40 (2016).